Instability-Assisted Direct Writing of Micro-Structured Fibers featuring Sacrificial Bonds

R. Passieux, L. Guthrie, S. Hosseini Rad, M. Lévesque, D. Therriault, F.P. Gosselin*

Renaud PASSIEUX

Leigh GUTHRIE

Somayeh HOSSEINI RAD

Martin LÉVESQUE

Daniel THERRIAULT

Frédérick P. GOSSELIN
2900, boul. Édouard-Montpetit
Campus de l'Université de Montréal
Montréal (Québec), H3T 1J4, Canada
Email : frederick.gosselin@polymtl.ca

Natural materials are often assembled into hierarchical microstructures, thus achieving far superior mechanical properties compared to the intrinsic properties of their constituents [1, 2, 3]. Toughening mechanisms involving sacrificial bonds and hidden lengths [4] are found in many biological materials such as muscle [5], bone [6], nacre [7] and spider silk [8]. As defined in reference [9], sacrificial bonds consist of chemical connections that break before the main structural molecular chain. The breakage of a sacrificial bond releases a so-called hidden length which then unfolds and carries the load. This hierarchical configuration contributes to the energy required for the stretching and fracture of the structural molecular chain. We seek to apply this molecular scale mechanism at the microscopic level by fabricating micro-structured fibers featuring sacrificial bonds (general overview available in the Supporting Video 1).

The toughening effect of structural hierarchy in natural materials has been emulated [2] in material microstructure by machining engineering materials such as silica [3, 10], or Poly(methyl methacrylate) (PMMA) [11] into significantly tougher microstructures. The advent of three-dimensional (3D) printing technologies (e.g., fused deposition modeling (FDM), UV-assisted and solvent-cast printing [12]) enabled new possibilities for tailoring the mechanical properties of micro-structured composite materials [13]. The traditional FDM approach consists in depositing fused filaments in a layer-by-layer fashion [14]. The printing parameters must be precisely tuned: the velocity of the thread coming out of the printing head must match the relative velocity of the deposition platform; otherwise the deposited filament can be stretched if the platform is too fast, or to become unstable and buckle due to compressive stress. This instability known as liquid rope coiling [15], leads to a pile of regular and circular coils, e.g., a viscous thread of honey falling from a spoon onto a toast. By moving the substrate onto which the viscous thread is

falling, a rich variety of squiggly instability patterns can be generated. Through experimental [16] and numerical [17] studies, viscous, inertial, gravitational and, to a lesser extent, capillary forces have been shown to influence the coiling frequency [18]. A similar instability has been observed by using elastic rods [19] instead of a viscous fluid, and helical polymeric fibers [20] have been produced with the liquid rope coiling by having a viscous cellulose solution fall into a moving coagulating bath.

In this article, the liquid rope coiling instability is adapted to melt and solvent cast printing approaches [21] to produce microstructured fibers with a one-step process. In the instability-assisted fused deposition modeling (IFDM) approach, a filament of Poly(Lactic Acid) (PLA) is fused and extruded before cooling and solidifying in ambient air. In the instability-assisted solvent cast printing approach (ISCP), a solution of PLA in dichloromethane is extruded in ambient air and solidifies as the solvent evaporates. Both approaches can be schematized as in **Figure 1a**: a polymeric filament is extruded at a speed V_t from a nozzle located at a distance H above a platform which moves perpendicularly at a constant speed V_p, with $V_t > V_p$ to give rise to the instability. Tuning of process parameters results in micro-structured fibers exhibiting a periodic pattern with contour length l_c, wavelength λ, and filament diameter d_f, as shown in Figure 1b.) Where the thread intersects itself, the material fuses and creates sacrificial bonds, i.e., bonds α and β in the schematic of Figure 1b. Upon testing a fiber in uniaxial tension (Figure 1b), a characteristic saw-tooth curve can be observed (Figure 1c). The first two peaks correspond to the breakage of bonds α and β, respectively. The last peak corresponds to the break of the core fiber also referred to as the backbone in analogy with the terminology of polymer chemistry. The dramatic drop of the force after the break of bonds α and β corresponds to the unwinding of the coiled loop length, referred to as the hidden length.

Fibers produced with both IFDM and ISCP for varying speed ratios V_t/V_p exhibit different patterns as shown in **Figure 2a**. The family portrait of the patterns resulting from both processes obtained with the same slenderness ratio ($H/d_f = 10$) are juxtaposed in order to underline their similarity despite their differences of scale, i.e., for IFDM $d_f = 0.5$ mm; for ISCP $d_f = 0.03$ mm. Straight fibers (━), meandering (▲), alternating (■), coiling (●), and overlapping (♦) patterns are successively produced by increasing V_t/V_p as observed in previous macroscopic experiments using Newtonian fluid [16, 22].

A process map (Figure 2b) inspired by the state diagram of reference [22] is produced in order to classify the observed patterns with respect to the speed and height settings. The map can be divided in different zones dominated by one specific pattern. When $V_t/V_p < 1$, the platform stretches the thread which may either break or result in a thinner straight fiber. When the thread speed equals the platform speed (i.e., $V_t/V_p = 1$) the thread remains linear and gives rise to a simple straight fiber (Figure 2b; ━). If the speed ratio V_t/V_p is slightly higher than one (Figure 2b; ▲) the accumulation of fluid induces a compressive force resulting in a bending instability; meandering patterns are thus produced. Speed ratios confined in a range between ~1.5 and ~2.5 may result in either coiling or alternating patterns (Figure 2b; ■). For $V_t/V_p > 2.5$ the coiling motion of the thread is similar to the simple rope coiling instability observable with a motionless platform. Coiling patterns with distinct loops (Figure 2b; ●) are first produced. Upon increasing $V_t/V_p > 4$ an overlapping pattern is obtained with a superposition of loops (Figure 2b; ♦).

Observations of the geometry of instability patterns emphasize the robustness of the liquid rope coiling instability. In Figure 2c, the wave number H/λ calculated for fibers produced with parameters ensuring that the coiling motion occurs in the viscous regime (see Supporting

Material 1) is reported as a function of the speed ratio V_t/V_p. By considering only coiling

patterns, H/λ increases linearly with V_t/V_p, as would be expected for a Newtonian fluid coiling

in the viscous regime [23]. Despite the many differences of scale and rheological properties

between the processes implemented in this work and in the literature [16, 22], the same deposition

patterns are obtained with predictable wavelengths. Thus, by appropriately choosing the

fabrication parameters, a predictable instability pattern can be selected.

Mechanical tensile tests were performed to determine the mechanical properties of the structured

fibers. In order to simplify the analysis, we define an apparent stress $\sigma^* = 4F/\pi d_f{}^2$ and an

apparent strain as $\varepsilon^* = 100 * \Delta L/l_0$, where F is the force applied by the tensile machine, d_f is

the mean diameter of the fiber backbone, ΔL the displacement of the clamps, and l_0 the initial

length of the fiber between the clamps. Finally, the specific modulus of toughness $U_T{}^*$ is

calculated as the energy of deformation divided by the weight of the fiber.

Representative tensile curves of a coiling pattern fiber made by IFDM and ISCP are shown in

Figure 3 a and **b,** respectively. The saw-tooth shape of the curve of the IFDM-made fiber

(Figure 3a) is associated with sacrificial bonds [24]. The events related to one bond are captured at

the top of Figure 3a with a sequence of photographs depicting bond breakage and hidden length

extension also visible in **Supporting video 4** (link to video 4). For example, at $\varepsilon^* = 75$ %, the

bond β must transmit the force applied to the fiber. At $\varepsilon^* = 83$ %, the bond reaches the

maximum stress it can hold (i.e., $\sigma^* = 22$ MPa) and breaks. The hidden length corresponding to

the broken bond is thus exposed and its unfolding corresponds to the apparent stress drop.

Around $\varepsilon^* = 125$ %, σ^* increases as the straightening of the hidden length becomes more

resistant. Since the bond β was the last one intact, its release is followed by the tensioning and

breakage of the backbone. The apparent ultimate strain of the fiber is then $\varepsilon^* = 137$ %. For the sake of comparison, the tensile test curve of a straight fiber produced at a speed ratio $V_t/V_p = 1$ is shown in green dotted line on Figure 3a. We notice that the backbone of the coiled fiber breaks at $\sigma^* = 40$ MPa whereas the straight fiber breaks at $\sigma^* = 66$ MPa. In general, similar observations can be made from Figure 3b which presents the tensile curve of a microscopic coiled fiber made by ISCP, containing 40 bonds, and a straight microfiber. The inset emphasizes the saw-tooth behavior due to bond breakage, which is also illustrated in **Supporting video 5** (link to video 5). Although qualitatively similar behaviors are observed in terms of sacrificial bonds for IFDM and ISCP, when comparing Figures 3a and 3b, the larger apparent strains observed for both straight and coiled ISCP fibers is significant. It is probably due to a size scale effect which makes PLA more ductile at smaller sizes.

We focus on tailoring the mechanical properties of the fibers and improving their toughness by microstructuring the material. In Figure 3c, the specific toughness of fiber specimens with different instability patterns made by IFDM at different speed ratios is reported. In Figure 3d, an Ashby plot [25] displays the apparent stiffness K_a, defined as $F/\Delta L$ at $\varepsilon^* = 3$ %, and the specific toughness of the fibers for each instability pattern. The Ashby plot highlights the possibilities of tailoring the mechanical properties of the produced fibers by choosing their instability pattern. Representative tensile curves for each pattern are shown in the **Supporting Material 3**. By spanning the range of instability patterns through a variation of V_t/V_p, we seek to find the best pattern to maximize the toughness enhancement in comparison with average toughness of straight fibers $\overline{U_T}^*_{Straight} = 1.6$ kJ/kg. On Figure 3 c and d, the coiling (●) and overlapping (♦) patterns exhibit noticeably lower specific toughness properties than the benchmark straight fiber (46% of $\overline{U_T}^*_{Straight}$ in both cases) because none of these fibers totally unfold before breaking.

Meandering patterns (▲) provide the largest gain in toughness on average (nearly 200%

of $\overline{U_T^*}_{Straight}$) despite the fact that they do not feature sacrificial bonds. Therefore, their

toughness enhancement in comparison to the benchmark straight fiber is only due to the energy

necessary to straighten the fiber. The meandering fibers, with their shape akin to that of a spring,

have very low stiffness ($K_a < 1$ MN/mm). They are very compliant and necessitate large strain

before absorbing energy. Alternating patterns (■) have considerable toughness (150%

of $\overline{U_T^*}_{Straight}$), although less than the meandering patterns. On the other hand, their sacrificial

bonds confer them significant rigidity (3.5 MN/mm $< K_a < 5.5$ MN/mm), and act as fuses

requiring reaching a threshold effective stress before they allow strain. It is noteworthy to

mention that in reference [4], when stretching proteins of aggrecan, the energy necessary to break

sacrificial bonds is little in comparison to the energy necessary to uncoil and stretch the hidden

length. Although the sacrificial bonds do not absorb a large amount of energy, they play a key

role: they stiffen the fiber by hiding part of its length until a sufficient load is applied on them.

The scatter in the toughness values obtained is large, especially so for the meandering and

alternating patterns. The best alternating specimens are more than twice as tough as the best

straight benchmark, but the worst alternating fiber is even worse than the benchmark. On the one

hand, this scatter indicates that we do not fully master all the complexity of the physics involved

in the fabrication process, but on the other it is revealing of the potential we could hope to

achieve by making only specimens with the best properties reliably. An interrelation between the

number of sacrificial bonds in the sample, the strength of the bonds relative to the backbone and

the varying slenderness of the patterns is possibly responsible of this scatter. Related to these

parameters, we noticed that the mode of rupture is not always the same, and some specimens fail

early before all sacrificial bonds are broken. Some early breakages are due to the presence of small defects induced by previous bond breakages and hidden lengths unwinding.

Understanding the cause of early breakage is a key for further optimization of the fiber production. Some possible causes are illustrated in **Figure 4**. A first possible cause is the stress concentration appearing at the site of a broken sacrificial bond. A small defect is observed in SEM images of a fiber produced via ISCP, taken before and after the breakage of a sacrificial bond (Figure 4 a, b). A second possible cause is the cusp appearing at the top of the loop during the unfolding of IFDM-made fibers, as observed on bright field microscopy images taken just after the breakage of a bond, and during the unfolding event (Figure 4 c-e). For these fibers of larger diameter, the unfolding can lead to the formation of a cusp at the top of the loop due to a combination of bending and torsion. This phenomenon seems to be dependent on the mechanically tested specimen. It is not understood yet and requires further investigation.

In summary, a fluid instability is harnessed and combined with two 3D printing techniques (IFDM, ISCP) in order to fabricate structured fibers featuring sacrificial bonds in a one-step process at different scales. The patterning technique allows the creation of sacrificial bonds whenever the fiber coils on itself, which confers rigidity and improved toughness to the material in an analogous fashion to many biological materials such as the spiral protein chains of spider silk. By varying the instability parameters, the mechanical properties of the fibers can be tailored to make them more or less rigid and more or less tough. Some optimization of the process is still necessary to minimize the possible creation of stress concentrations resulting from bond breakage or unfolding events which weaken the backbone and can lead to premature fiber

failure. This optimization is far from trivial as the system is highly coupled: varying the printing head speed or height not only influences the fluid instability, it also affects the cooling or evaporating time and thus the sacrificial bond strength as well as the shear in the extruded polymeric fluid and thus the alignment of the molecules. Nevertheless, the one-step characteristic of the proposed processes, the low energy and low pressure (less than 4.2 MPa) required in ISCP, and the simplicity to implement IFDM with an off-the-shelf 3D-printer are significant advantages for fast adoption. The approach is adaptable to any material which can be dissolved or melted to make it flow. Thus the process could be transposed to high performance polymers such as aramid and nylon, or the multitude of materials used in FDM, or even to shape nanotubes[26]. Additionally, for applications such as scaffold printing for tissue growth where material selection is limited because of requirements of biocompatibility and printability, the option to microstructure the material via instability-assisted fabrication could broaden the range of effective stiffness and toughness available to designers. Parallels can be drawn between fibers made by instability-assisted fabrication and nonwoven materials made by consolidating disordered fibers or by electrospinning. In the fibers tested here, the sacrificial bonds link the fiber to itself in an orderly fashion, whereas in nonwoven materials the bonds link the fibers together in a random fashion. In both cases the bonds play a crucial role in the mechanical properties of the structure and its energy-absorption capability [27]. Finally, to complete the analogy with the spider which creates different silks for different purposes, the many instability patterns could be organized in a web-like architecture to create a truly hierarchical structure with high energy absorption and damage tolerance qualities [28].

Experimental Section

a) Instability-assisted fused deposition modeling (IFDM)

A filament of Poly(Lactic Acid) (PLA) (MakerBot PLA orange) is fused at 230°C. At this temperature, the PLA viscosity is approximately ~260 Pa·s [29]. The filament is extruded through the printing head of a commercial 3D printer (MakerBot replicator) as illustrated in **Supporting Video 2** (link to video 2). The thread has a diameter $d_f = 500$ µm and is extruded at a constant speed $V_t = 30$ mm · s^{-1}. The thread solidifies as it cools in the ambient air (22°C) and is collected by a conveyor belt moving at a speed V_p. The deposition height H of the nozzle can be set between 5 to 50 mm by raising or lowering the support of the conveyor.

b) Instability-assisted solvent-cast printing (ISCP)

The fluid extruded is a 25 w_t% solution of PLA (grade 4032D, Nature works LLC, molecular weight $M_w = 207$ kg·mol^{-1}) dissolved in dichloromethane (DCM) (Sigma-Aldrich), a volatile solvent. After mixing the PLA in the DCM in a 20 mL sealed glass bottle, the solution is stored for 48h for complete dissolution to occur. The apparent viscosity of the shear-thinning solution varies from 10 to 50 Pa·s depending on the pressure applied in the process [30]. The PLA solution is extruded at a speed V_t through a 30 µm diameter pre-pulled glass needle (WPI, Pulled glass 30 µm) held by a computer-controlled robot (I&J2200-4, I&J Fisnar), as illustrated in **Supporting Video 3** (link to video 3). A pressure ranging between 350 kPa and 840 kPa is necessary to extrude the polymeric fluid at speeds between 2 mm · s^{-1} and about 10 mm · s^{-1}. Die swell effect and volume loss through solvent evaporation result in a fiber diameter d_f different from that of the needle. The deposition height H is varied in a range between 200 to 500 µm. The thread solidifies via fast evaporation of the solvent and is collected onto a microscope glass slide (Fisherbrand) which is translating at a constant speed of $V_p = 2$ mm · s^{-1} using the same robotic system.

c) Batches production and Mechanical tests

Six batches of fibers are produced either by IFDM or by ISCP in order to perform mechanical

tests using an electromechanical machine (Insight MTS 50KN) with a 1000 N load cell for fibers

produced via IFDM and a 5 N load cell for the smaller fibers produced via ISCP. Mechanical

tests are repeated seven times for each set of parameters. Settings relative to the production and

to the tensile testing of the batches are listed in Supporting Material 4.

Supporting Information
Supporting Information is available from the Wiley Online Library or from the author.

REFERENCES

[1]   U. G. Wegst, H. Bai, E. Saiz, A. P. Tomsia, R. O. Ritchie, Nature materials 2015, 14, 23; M. A. Meyers, J. McKittrick, P.-Y. Chen, Science 2013, 339, 773.
[2]   Q. Chen, N. M. Pugno, Journal of the Mechanical Behavior of Biomedical Materials 2013, 19, 3.
[3]   D. Sen, M. J. Buehler, Sci. Rep. 2011, 1.
[4]   G. E. Fantner, E. Oroudjev, G. Schitter, L. S. Golde, P. Thurner, M. M. Finch, P. Turner, T. Gutsmann, D. E. Morse, H. Hansma, P. K. Hansma, Biophysical Journal 2006, 90, 1411.
[5]   P. E. Marszalek, H. Lu, H. Li, M. Carrion-Vazquez, A. F. Oberhauser, K. Schulten, J. M. Fernandez, Nature 1999, 402, 100.
[6]   G. E. Fantner, T. Hassenkam, J. H. Kindt, J. C. Weaver, H. Birkedal, L. Pechenik, J. A. Cutroni, G. A. G. Cidade, G. D. Stucky, D. E. Morse, P. K. Hansma, Nature Materials 2005, 4, 612.
[7]   B. L. Smith, T. E. Schaffer, M. Viani, J. B. Thompson, N. A. Frederick, J. Kindt, A. Belcher, G. D. Stucky, D. E. Morse, P. K. Hansma, Nature 1999, 399, 761.
[8]   N. Becker, E. Oroudjev, S. Mutz, J. P. Cleveland, P. K. Hansma, C. Y. Hayashi, D. E. Makarov, H. G. Hansma, Nature materials 2003, 2, 278.
[9]   A. E. Elbanna, J. M. Carlson, PLoS ONE 2013, 8, 56118.
[10]   M. Mirkhalaf, A. K. Dastjerdi, F. Barthelat, Nature communications 2014, 5.
[11]   F. Barthelat, Bioinspiration & biomimetics 2010, 5, 035001.
[12]   S.-Z. Guo, F. Gosselin, N. Guerin, A.-M. Lanouette, M.-C. Heuzey, D. Therriault, Small 2013, 9, 4090; L. L. Lebel, B. Aissa, M. A. E. Khakani, D. Therriault, Advanced Materials 2010, 22, 592.
[13]   R. D. Farahani, H. Dalir, B. Aissa, M. A. El Khakani, M. Lévesque, D. Therriault, Composites Part A: Applied Science and Manufacturing 2011, 42, 1910; R. D. Farahani, M. Pahlavanpour, H. Dalir, B. Aissa, M. A. E. Khakani, M. Lévesque, D. Therriault, Materials & Design 2012, 41, 214.
[14]   S. S. Crump, Google Patents 1992.
[15]   G. Barnes, R. Woodcock, American Journal of Physics 1958, 26, 205.
[16]   S. CHIU-WEBSTER, J. R. LISTER, Journal of Fluid Mechanics 2006, 569, 89; R. L. Welch, B. Szeto, S. W. Morris, Physical Review E 2012, 85, 066209.
[17]   N. M. Ribe, J. R. Lister, S. Chiu-Webster, Physics of Fluids 2006, 18; P.-T. Brun, N. M. Ribe, B. Audoly, Physics of Fluids (1994-present) 2012, 24.
[18]   N. M. Ribe, M. Habibi, D. Bonn, Annual Review of Fluid Mechanics 2012, 44, 249.
[19]   M. K. Jawed, P. M. Reis, Extreme Mechanics Letters 2014.
[20]   B. Jia, L. Yu, F. Fu, L. Li, J. Zhou, L. Zhang, RSC Advances 2014, 4, 9112.
[21]   J. Ren, in *Biodegradable Poly(Lactic Acid): Synthesis, Modification, Processing and Applications*, Springer Berlin Heidelberg, 2010, 142; B. Gupta, N. Revagade, J. Hilborn, Progress in Polymer Science 2007, 32, 455.
[22]   S. W. Morris, J. H. P. Dawes, N. M. Ribe, J. R. Lister, Physical Review E 2008, 77, 066218.
[23]   M. Maleki, M. Habibi, R. Golestanian, N. M. Ribe, D. Bonn, Physical Review Letters 2004, 93, 214502.
[24]   T. M. Dugdale, R. Dagastine, A. Chiovitti, P. Mulvaney, R. Wetherbee, Biophysical Journal 2005, 89, 4252.
[25]   M. Ashby, Materials Selection in Mechanical Design 1999.
[26]   N. Geblinger, A. Ismach, E. Joselevich, Nat Nano 2008, 3, 195.
[27]   A. Ridruejo, C. González, J. Llorca, International Journal of Solids and Structures 2011, 48, 153.
[28]   S. W. Cranford, A. Tarakanova, N. M. Pugno, M. J. Buehler, Nature 2012, 482, 72.
[29]   N. Othman, in *Chemical and Biological Engineering*, Vol. doctor oh philosophy, University of British Columbia, Vancouver 2012.
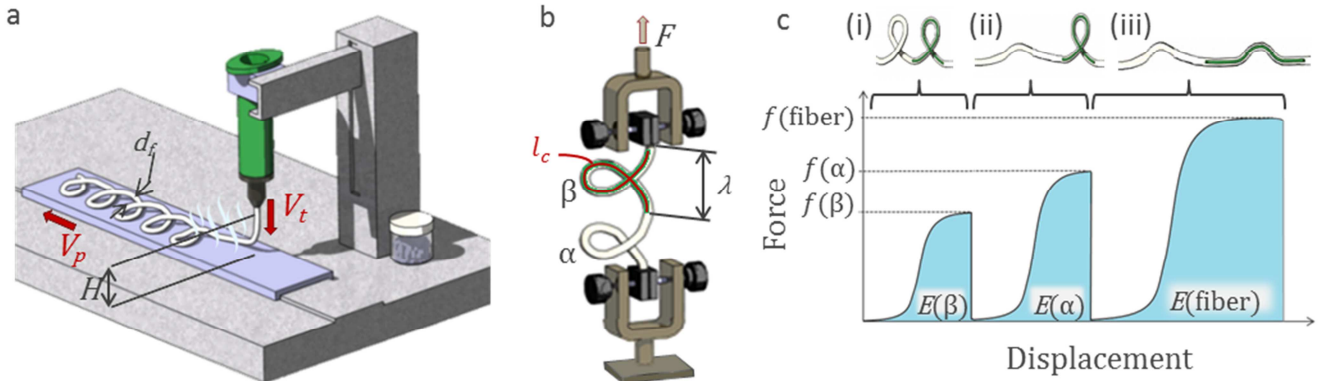[30]   S.-Z. Guo, M.-C. Heuzey, D. Therriault, Langmuir 2014, 30, 1142.

Figure 1: Schematic general view of the process a) Schematic representation of the deposition process which variables are the deposition height H, fiber diameter d_f, extrusion speed V_t, and platform speed V_p. The thread is coiled by a fluid instability and solidifies by solvent evaporation or polymer cooling. b) The produced fibers are characterized by a contour length l_c and a periodicity length λ. The behavior of fibers with sacrificial bonds (α, β) is characterized via tensile tests. c) Sacrificial bonds breakage and hidden length unfolding events are illustrated with a schematic and result in a characteristic saw-tooth tensile curve. First two peaks correspond to the breakage of bonds α and β when the force reaches their resistance value ($f(\alpha)$, $f(\beta)$). The drops of force correspond to the unfolding of loops. The last peak corresponds to the break of the backbone once the fiber has unfolded. The energy absorbed by the breakage of the bonds and unfolding of loops $E(\alpha)$ and $E(\beta)$ is added to the energy absorbed by the breakage of the unfolded backbone $E(backbone)$.
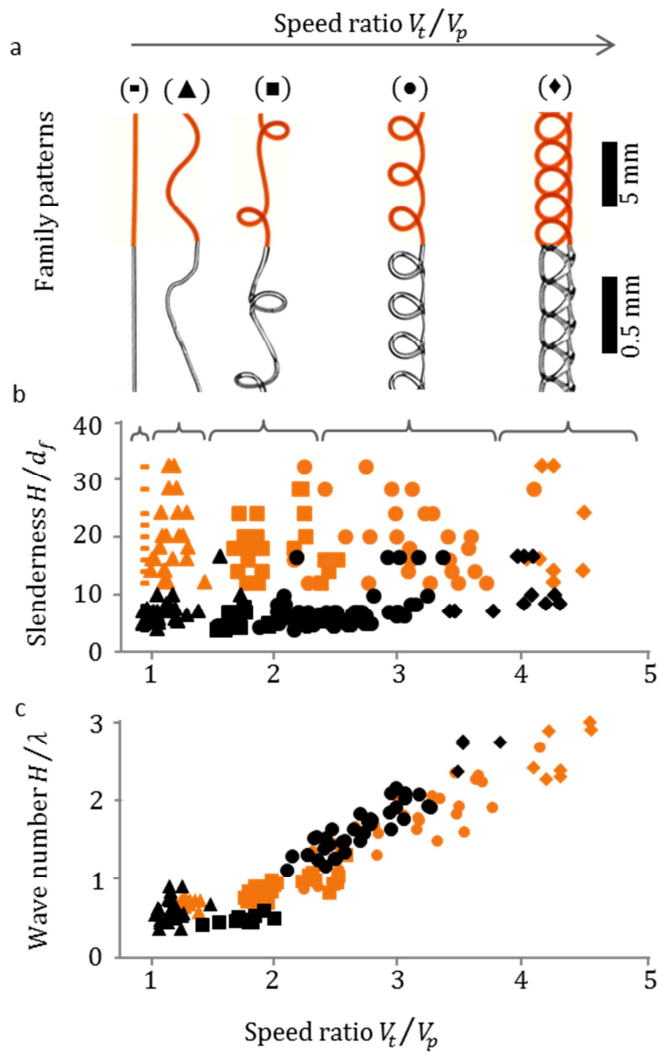
Figure 2: a). Photographs of PLA fibers resulting from batches A-IFDM (orange) and E-ISCP (black), produced for the same slenderness ($H/d_f = 10$). Straight fibers (—), meandering (▲), alternating (■), coiling (•), and overlapping (♦) patterns are successively produced by increasing the speed ratio from 1 to 5. b) Process map defining the zones of predominance of each pattern depending on process parameters. c) Wave number (H/λ) of coiling fibers as a function of the speed ratio V_t/V_p
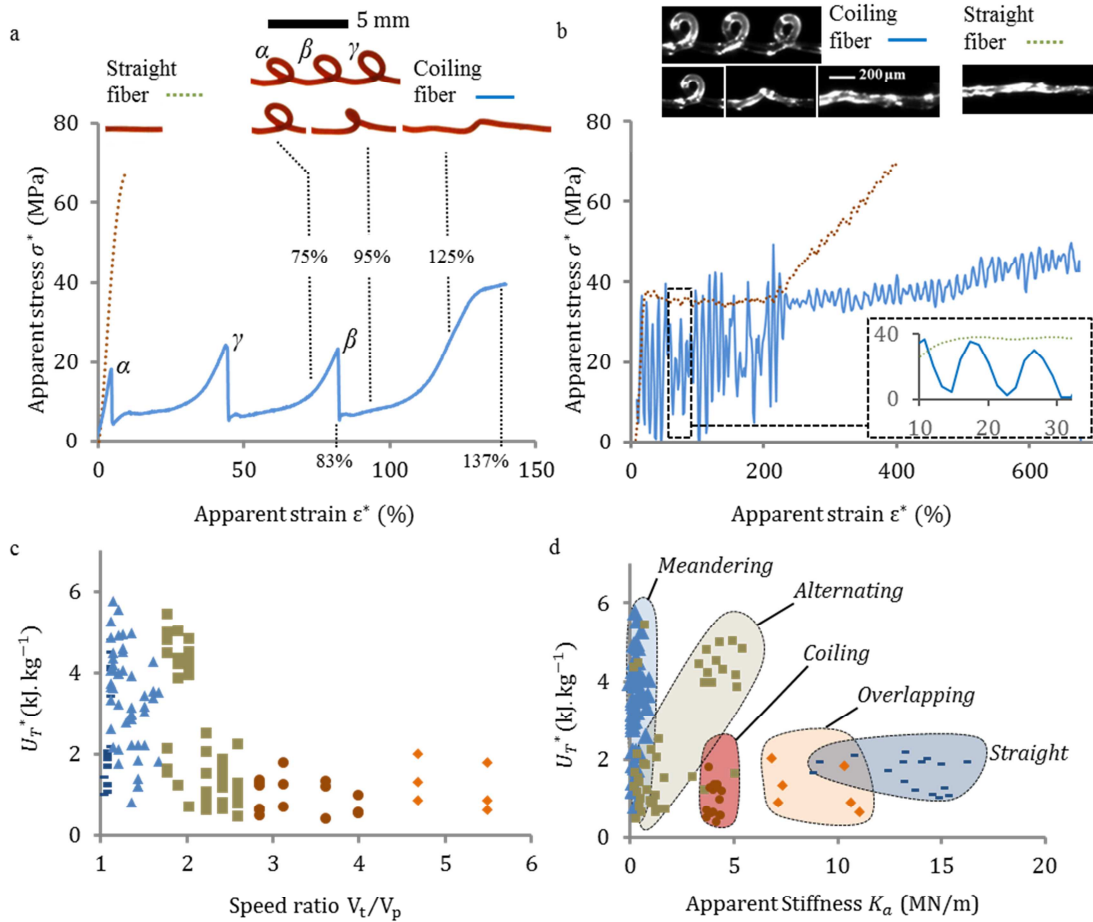
Figure 3: Tensile tests are performed on squiggly PLA fibers from: a) batch C-IFDM and b) batch F-ISCP. The sequences of sacrificial bond breakage and hidden length extension events are illustrated by photographs and result in characteristic saw-tooth curves (solid line) in the apparent stress strain plot. Representative tensile curves of straight fibers (dash line) act as benchmark for the two processes. Mechanical properties of IFDM made fibers are analyzed and plot with respect to their pattern. c) Plot of the specific toughness of IFDM made fibers ($H/d_f = 18$), depending on the speed ratio. Symbols represent the different instability patterns as defined in Figure 2. d) Ashby plot of U_T^* with respect to the apparent stiffness K_a of the fibers. Performances of each pattern are approximatively delimited by colored zones.
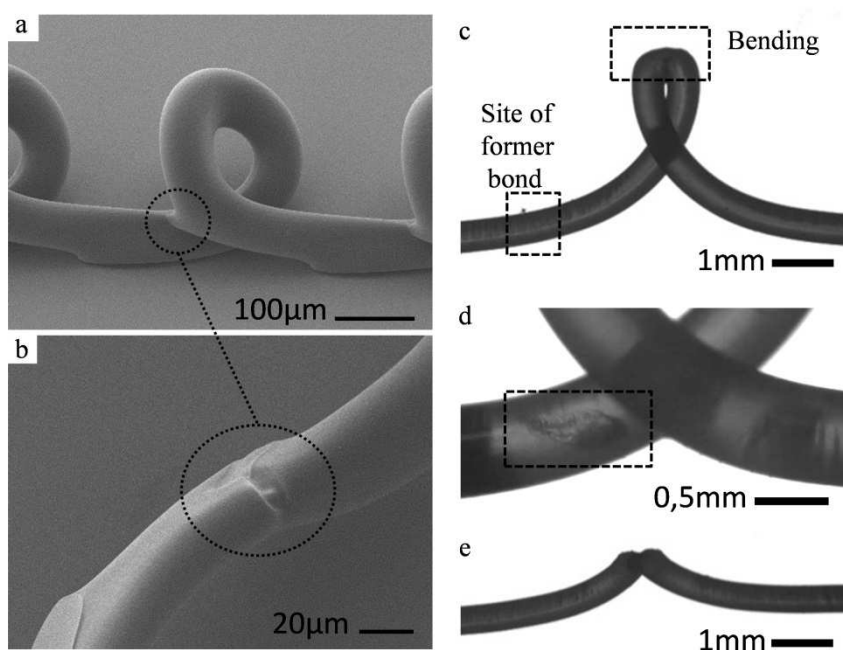
Figure 4: Illustration of the causes of early break of fibers produced via ISCP (a, b) and via IFDM (c, d, e): a) SEM photograph of a loop with a visible sacrificial bond; e) defect induced at the former place of the broken bond; c) bright field microscopy images of a loop just after a bond breakage; d) of the defect created at the place where the bond was formed; e) and of the loop at an advanced stage of the unfolding where the defect created at the top of the former loop is visible